CMU-HEP00-03
UTPT-00-07
August 2000

NRQCD Analysis of Bottomonium Production at the Tevatron

Eric Braaten
Physics Department, Ohio State University, Columbus, OH 43210, USA

Sean Fleming
Physics Department, University of Toronto, Ontario, M5S 1A7, Canada

Adam K. Leibovich
Department of Physics, Carnegie Mellon University, Pittsburgh, PA 15213, USA

Abstract

Recent data from the CDF collaboration on the production of spin-triplet bottomonium states at the Tevatron $p\bar{p}$ collider are analyzed within the NRQCD factorization formalism. The color-singlet matrix elements are determined from electromagnetic decays and from potential models. The color-octet matrix elements are determined by fitting the CDF data on the cross sections for $\Upsilon(1S)$, $\Upsilon(2S)$, and $\Upsilon(3S)$ at large p_T and the fractions of $\Upsilon(1S)$ coming from $\chi_b(1P)$ and $\chi_b(2P)$. We use the resulting matrix elements to predict the cross sections at the Tevatron for the spin-singlet states $\eta_b(nS)$ and $h_b(nP)$. We argue that $\eta_b(1S)$ should be observable in Run II through the decay $\eta_b \to J/\psi + J/\psi$.

I. INTRODUCTION

The NRQCD factorization formalism provides a systematic framework for analyzing the inclusive production of heavy quarkonium [1]. Long-distance effects involving the binding of a heavy quark-antiquark pair into quarkonium are factored into parameters called NRQCD matrix elements. These nonperturbative parameters are universal, so values extracted from one high energy physics experiment can be used to predict the production rate in others. The NRQCD matrix elements scale as definite powers of v, where v is the typical relative velocity of the heavy quark. The NRQCD factorization approach becomes phenomenologically useful upon truncating the expansion in v so as to reduce the independent NRQCD matrix elements to a manageable number. The truncation is most reliable for the heaviest quarkonium states, namely the $b\bar{b}$ system for which v^2 is roughly 1/10.

The most abundant source of data on bottomonium production is the Tevatron $p\bar{p}$ collider. In Run IA of the Tevatron, the CDF collaboration was able to resolve the individual S-wave bottomonium states $\Upsilon(1S)$, $\Upsilon(2S)$, and $\Upsilon(3S)$ and measure their production cross sections [2]. An analysis of the CDF data within the NRQCD factorization formalism was carried out by Cho and Leibovich [3]. The analysis is complicated by the production of P-wave bottomonium states that subsequently make transitions to S-wave states. Cho and Leibovich found that the CDF data was insufficient to determine all the important NRQCD matrix elements and they had to make educated guesses for some of them.

The CDF collaboration has recently analyzed the data on bottomonium production from Run IB at the Tevatron. In addition to much higher statistics on the cross sections for $\Upsilon(1S)$, $\Upsilon(2S)$, and $\Upsilon(3S)$ [4], they also have results on the production of the P-wave states $\chi_b(1P)$ and $\chi_b(2P)$ [5]. The high quality of the new CDF data justifies an updated theoretical analysis, with careful attention to the experimental and theoretical errors.

In this paper, we present a quantitative analysis of the new CDF data on bottomonium production within the NRQCD factorization formalism. The color-singlet NRQCD matrix elements for S-wave states are determined from their electromagnetic decays, while those for P-wave states are estimated from potential models. The color-octet NRQCD matrix elements are determined by fitting the CDF data, taking full account of the feeddown from transitions between bottomonium states. The resulting values of the matrix elements are used to predict the cross sections for the spin-triplet and spin-singlet bottomonium states in Run II of the Tevatron.

II. NRQCD MATRIX ELEMENTS

The NRQCD factorization approach provides a model-independent framework for analyzing the inclusive production of heavy quarkonium [1]. The factorization formula for the differential cross section for the inclusive production of a bottomonium state H of momentum P has the schematic form

$$d\sigma[H(P)] \;=\; \sum_n d\sigma[b\bar{b}(n,P)]\langle O^H(n)\rangle, \tag{1}$$

where the sum extends over both color-singlet and color-octet and over all angular momentum channels for the $b\bar{b}$ pair. The $b\bar{b}$ cross sections, which are independent of the bottomonium state H, can be calculated using perturbative QCD. All dependence on the state H is

factored into parameters $\langle O^H(n)\rangle$ called *NRQCD matrix elements*. These phenomenological parameters can be expressed as matrix elements in an effective field theory called nonrelativistic QCD (NRQCD). A nonperturbative analysis of NRQCD reveals how the various matrix elements scale with the typical relative velocity v of the heavy quark in quarkonium. Spin symmetry, which is an approximate symmetry of QCD, also gives relations between various matrix elements.

The relative importance of the terms in the factorization formula (1) depends on the size of the $b\bar{b}$ cross sections and on the size of the matrix elements. According to the velocity-scaling rules, the most important matrix element for direct $\Upsilon(1S)$ production is the color-singlet parameter $\langle O_1^{\Upsilon(1S)}({}^3S_1)\rangle$. The spin-symmetry relations can be used to reduce the next most important matrix elements to three color-octet parameters: $\langle O_8^{\Upsilon(1S)}({}^3S_1)\rangle$, $\langle O_8^{\Upsilon(1S)}({}^1S_0)\rangle$, and $\langle O_8^{\Upsilon(1S)}({}^3P_0)\rangle$. These color-octet matrix elements are important, because the cross sections for producing color-octet $b\bar{b}$ pairs can be much larger than for color-singlet $b\bar{b}$ pairs. There are analogous matrix elements that describe the direct production of $\Upsilon(2S)$ and $\Upsilon(3S)$. The NRQCD factorization formula (1) for direct $\Upsilon(nS)$ production reduces to

$$\begin{aligned} d\sigma[\Upsilon(nS)] = {} & d\sigma[b\bar{b}_1({}^3S_1)]\langle O_1^{\Upsilon(nS)}({}^3S_1)\rangle + d\sigma[b\bar{b}_8({}^3S_1)]\langle O_8^{\Upsilon(nS)}({}^3S_1)\rangle \\ & + d\sigma[b\bar{b}_8({}^1S_0)]\langle O_8^{\Upsilon(nS)}({}^1S_0)\rangle + \left(\sum_J (2J+1)\, d\sigma[b\bar{b}_8({}^3P_J)]\right)\langle O_8^{\Upsilon(nS)}({}^3P_0)\rangle. \end{aligned} \quad (2)$$

The factor of $2J+1$ in the last term comes from using a spin-symmetry relation to eliminate $\langle O_8^{\Upsilon(nS)}({}^3P_J)\rangle$ in favor of $\langle O_8^{\Upsilon(nS)}({}^3P_0)\rangle$.

The most important matrix elements for the direct production of the P-wave states $\chi_{bJ}(1P)$, $J = 0, 1, 2$, can be reduced to a color-singlet parameter $\langle O_1^{\chi_{b0}(1P)}({}^3P_0)\rangle$ and a single color-octet parameter $\langle O_8^{\chi_{b0}(1P)}({}^3S_1)\rangle$. There are analogous matrix elements that describe the direct production of $\chi_{bJ}(2P)$ and $\chi_{bJ}(3P)$. The NRQCD factorization formula (1) for direct $\chi_{bJ}(nP)$ production reduces to

$$d\sigma[\chi_{bJ}(nP)] = d\sigma[b\bar{b}_1({}^3P_J)]\langle O_1^{\chi_{bJ}(nP)}({}^3P_J)\rangle + (2J+1)\, d\sigma[b\bar{b}_8({}^3S_1)]\langle O_8^{\chi_{b0}(nP)}({}^3S_1)\rangle. \quad (3)$$

In the last term, the factor of $2J+1$ comes from using a spin-symmetry relation to eliminate $\langle O_8^{\chi_{bJ}(nP)}({}^3S_1)\rangle$ in favor of $\langle O_8^{\chi_{b0}(nP)}({}^3S_1)\rangle$. We can also use a spin-symmetry relation to replace $\langle O_1^{\chi_{bJ}(nP)}({}^3P_J)\rangle$ in the first term by $(2J+1)\langle O_1^{\chi_{b0}(nP)}({}^3P_0)\rangle$. The matrix elements for $\Upsilon(nS)$ and $\chi_{bJ}(nP)$ enumerated above should be sufficient for a quantitative description of the production of S-wave and P-wave bottomonium states.

The NRQCD factorization formula gives the cross section for the *direct* production of a given bottomonium state. The cross sections that are most easily measured in experiments are *inclusive* cross sections that include contributions from the direct production of higher bottomonium states which subsequently decay into the given state. For example, the feeddown from $\chi_b(1P)$, $\Upsilon(2S)$, and $\chi_b(2P)$ accounts for roughly 27%, 11%, and 11% of the $\Upsilon(1S)$ cross section, respectively [5]. Taking into account the feeddown from higher $\Upsilon(mS)$ and $\chi_{bJ}(mP)$ states, the cross section for inclusive $\Upsilon(nS)$ production can be written

$$\begin{aligned} d\sigma[\Upsilon(nS)]_{\rm inc} = {} & d\sigma[b\bar{b}_1({}^3S_1)]\langle O_1({}^3S_1)\rangle_{\rm inc}^{\Upsilon(nS)} + \sum_J d\sigma[b\bar{b}_1({}^3P_J)]\langle O_1({}^3P_J)\rangle_{\rm inc}^{\Upsilon(nS)} \\ & + d\sigma[b\bar{b}_8({}^3S_1)]\langle O_8({}^3S_1)\rangle_{\rm inc}^{\Upsilon(nS)} + d\sigma[b\bar{b}_8({}^1S_0)]\langle O_8({}^1S_0)\rangle_{\rm inc}^{\Upsilon(nS)} \end{aligned}$$

	$\Upsilon(3S)$	$\chi_{b2}(2P)$	$\chi_{b1}(2P)$	$\chi_{b0}(2P)$	$\Upsilon(2S)$	$\chi_{b2}(1P)$	$\chi_{b1}(1P)$	$\chi_{b0}(1P)$	$\Upsilon(1S)$
$\chi_{bJ}(3P)$	0 ?	0 ?	0 ?	0 ?	0 ?	0 ?	0 ?	0 ?	0 ?
$\Upsilon(3S)$	1	11.4±0.8	11.3±0.6	5.4±0.6	10.6±0.8	0.6±0.1	0.6±0.1	0.4±0.1	11.2±0.5
$\chi_{b2}(2P)$		1			16.2±2.4	1.1±0.2	1.1±0.2	0.7±0.2	12.1±1.3
$\chi_{b1}(2P)$			1		21±4	1.4±0.3	1.4±0.3	0.9±0.3	15.0±1.8
$\chi_{b0}(2P)$				1	4.6±2.1	0.3±0.1	0.3±0.1	0.2±0.1	2.3±0.9
$\Upsilon(2S)$					1	6.6±0.9	6.7±0.9	4.3±1.0	31.1±1.6
$\chi_{b2}(1P)$						1			22±4
$\chi_{b1}(1P)$							1		35±8
$\chi_{b0}(1P)$								1	< 6

TABLE I. Inclusive branching fractions $B_{H\to H'}$ (in %) for transitions between spin-triplet bottomonium states. The entries "0 ?" in the first row indicate that the feeddown from $\chi_{bJ}(3P)$ is neglected in our analysis.

$$+\left(\sum_J (2J+1) d\sigma[b\bar{b}_8(^3P_J)]\right) \langle O_8(^3P_0)\rangle_{\rm inc}^{\Upsilon(nS)}, \tag{4}$$

where the "inclusive NRQCD matrix elements" are

$$\langle O[n]\rangle_{\rm inc}^{\Upsilon(nS)} \;=\; \sum_H B_{H\to\Upsilon(nS)} \langle O^H[n]\rangle. \tag{5}$$

The sum over H includes $\Upsilon(nS)$ and all higher bottomonium states that can make transitions to $\Upsilon(nS)$. The coefficient $B_{H\to H'}$ is the inclusive branching fraction for H to decay into H'. By convention, we define $B_{H\to H} = 1$. The inclusive branching fraction for the observed bottomonium states are collected in Table I. These numbers were obtained by combining the measured branching fractions for the exclusive decays $\Upsilon(nS) \to \chi_{bJ}(mP)+\gamma$, $\chi_{bJ}(nP) \to \Upsilon(mS)+\gamma$, and $\Upsilon(nS) \to \Upsilon(mS)+\pi\pi$, with the exception of $B_{\Upsilon(3S)\to\Upsilon(1S)}$, which is a direct measurement [6].

In Table I, we have not included the spin-singlet states $\eta_b(nS)$ and $h_b(nP)$, which have yet to be observed. Transitions between spin-singlet and spin-triplet states are suppressed, because they proceed through magnetic $\Delta S = 1$ transitions. The rates for $\Delta S = 1$ transitions are suppressed relative to those for $\Delta S = 0$ transitions by a factor of v^2, which is roughly an order of magnitude. The branching fractions for $\eta_b(2S)$ into other bottomonium states are further suppressed by its large annihilation width into two gluons. Quantitative estimates of the electromagnetic and hadronic transition rates are given in Refs. [7,8]. They support the conclusion that the branching fractions for decays of spin-singlet states into spin-triplet states can be neglected.

The tiny branching fractions in Table I for the transition $\chi_{bJ}(2P) \to \chi_{bJ'}(1P)$ are the contributions from the double radiative transitions via $\Upsilon(2S)$. We have not included the contributions from the two-pion decays $\chi_{bJ}(2P) \to \chi_{bJ'}(1P) + \pi\pi$, which have not been observed. We can estimate their magnitude by observing that the rates for $\Upsilon(3S) \to \Upsilon(2S)+\pi\pi$ and $\Upsilon(3S) \to \Upsilon(2S)+\gamma\gamma$ are equal to within experimental errors. Since the phase space

available for the transitions $\chi_{bJ}(2P) \to \chi_{bJ'}(1P)$ is similar to that for $\Upsilon(3S) \to \Upsilon(2S)$, we expect the rate for $\chi_{bJ}(2P) \to \chi_{bJ'}(1P) + \pi\pi$ to be comparable to that for $\chi_{bJ}(2P) \to \chi_{bJ'}(1P) + \gamma\gamma$. Including the effects of two-pion transitions could increase the branching fraction for $\chi_{bJ}(2P) \to \chi_{bJ'}(1P)$ by a factor of 2 or 3, but since the values of $B_{\chi_{bJ}(2P)\to\chi_{bJ'}(1P)}$ in Table I are all less than 1.5%, they should still be negligible.

As indicated by the entries "0 ?" in the first row of Table I, we neglect the feeddown from the $\chi_b(3P)$ states, which have not been observed. A naive extrapolation from the other entries of the Table suggest that the branching fractions for $\chi_{b1}(3P)$ and $\chi_{b2}(3P)$ into $\Upsilon(3S)$ could be about 12%, while their branching fractions into $\Upsilon(1S)$ could be about 7%. These are small enough that they would not have a significant effect on our analysis. We have also neglected the feeddown from D-wave states.

III. PARTON DIFFERENTIAL CROSS SECTIONS

In hadron collisions, bottomonium with transverse momentum p_T of order m_b or larger is produced, at leading order in α_s, by parton *fusion* processes $ij \to b\bar{b} + k$. The differential cross section for producing a bottomonium state H with momentum P can be expressed in the schematic form

$$d\sigma[H(P)]_{\rm fusion} \;=\; f_{i/p} \otimes f_{j/\bar{p}} \otimes d\hat{\sigma}[ij \to b\bar{b}(P,n) + k]\langle O^H(n)\rangle, \tag{6}$$

where there is an implied sum over the partons i, j, k and over the $b\bar{b}$ channels n.

The order-α_s^3 fusion cross section in (6) gives a good first approximation only if the transverse momentum is not too much larger or too much smaller than m_b. For $p_T \gg m_b$, the order-α_s^3 fusion cross section for the channel $b\bar{b}_8(^3S_1)$ has the scaling behavior $d\hat{\sigma}/dp_T^2 \sim 1/p_T^4$, while all other channels are suppressed by powers of m_b^2/p_T^2 at leading order. Parton processes with scaling behavior are called *fragmentation* processes. The fragmentation contributions to $b\bar{b}$ channels other than $b\bar{b}_8(^3S_1)$ enter at higher order in α_s. The order-α_s^3 fusion cross sections therefore underestimate the $b\bar{b}$ cross section in these channels at large p_T. However, the CDF data on bottomonium production extends only out to $p_T = 20$ GeV [4], which is not large enough for fragmentation effects to dominate. In extracting the NRQCD matrix elements from that data, it should therefore be sufficient to use the fusion cross section (6).

The order-α_s^3 fusion cross section in (6) also fails at small p_T. For some $b\bar{b}$ channels, including $b\bar{b}_8(^1S_0)$ and $b\bar{b}_8(^3P_{0,2})$, there is an order-α_s^2 fusion cross section from the parton process $ij \to b\bar{b}$, which produces a $b\bar{b}$ pair with $p_T = 0$. In these channels, the order-α_s^3 fusion cross sections $d\sigma/dp_T^2$ diverge like $1/p_T^2$ as $p_T \to 0$. The divergence in the integral of the cross section for $ij \to b\bar{b} + k$ is cancelled by the radiative corrections to the cross section for $ij \to b\bar{b}$, so that the cross section integrated over p_T is finite order by order in α_s. In order to obtain a smooth prediction for $d\sigma/dp_T^2$ in the small p_T region, it is necessary to resum higher order corrections involving soft-gluon radiation. This resummation will have a significant effect on the shape of the p_T distribution, and therefore on the values of the NRQCD matrix elements used to fit that distribution. We will avoid the complications due to soft-gluon radiation at small p_T by using only the data from $p_T > 8$ GeV to fit the NRQCD matrix elements.

We proceed to describe each of the factors in the fusion cross section (6) in more detail. We include the contributions from the following combinations of colliding partons: $ij = gg$, gq, $g\bar{q}$, $q\bar{q}$, where $q = u, d, s, c$. The parton distributions $f_{i/p}(x_1, \mu_F)$ and $f_{j/\bar{p}}(x_2, \mu_F)$, which specify the momenta of the colliding partons, depend on a factorization scale μ_F. We will consider the CTEQ5L and MRST98LO parton distribution functions. They are both obtained from leading order analyses, and thus can be used consistently with leading order parton cross sections. Explicit expressions for the parton differential cross sections $d\hat{\sigma}$ are given in Ref. [3] and in Ref. [9]. They are proportional to $\alpha_s^3(\mu_R)$, where μ_R is the renormalization scale, and they depend on the mass m_b of the bottom quark. As part of the theoretical error, we will allow μ_F and μ_R to vary by factors of 2 from the central values $\mu_T = (m_b^2 + p_T^2)^{1/2}$. This central value interpolates between half the partonic invariant mass at $b\bar{b}$ threshold and half the partonic invariant mass at large p_T and central rapidity.

The cross sections also depend on two fundamental QCD parameters: α_s and m_b. We take the QCD coupling constant $\alpha_s(\mu)$ to run according to the one-loop formula, with the boundary value appropriate to the parton distribution function that is being used. For CTEQ5L, the coupling constant satisfies $\alpha_s(M_Z) = 0.127$ and $\alpha_s(m_b) = 0.232$. For MRST98LO, the coupling constant satisfies $\alpha_s(M_Z) = 0.125$ and $\alpha_s(m_b) = 0.226$.

The other fundamental QCD parameter in our calculation is the bottom quark mass m_b. There have been several recent determinations of m_b using sum rules calculated to next-to-next-to-leading order accuracy with nonrelativistic resummation [10]. A useful summary of these results is given by Beneke in Ref. [11]. The value of the pole mass is rather unstable under radiative corrections compared to short-distance definitions of the mass, such as the running mass evaluated at its own scale, $\bar{m}_b = m_b(\bar{m}_b)$. Beneke's best estimate for this mass is $\bar{m}_b = 4.23 \pm 0.08$ GeV. The definition of $\bar{m}_b$ is purely mathematical in character and not related to any physical thresholds involving the b quark. Two definitions that are also relatively stable under radiative corrections and whose definitions are related to thresholds in the bottomonium system are the 1S mass, which is the perturbative energy of the lowest bound state, and the PS mass, which is the sum of the pole mass and some energy related to the potential between the b and $\bar{b}$. Beneke's best estimates for these masses are $m_{b,1S} = 4.77 \pm 0.11$ GeV and $m_{b,PS}(2\,\mathrm{GeV}) = 4.57 \pm 0.10$ GeV. The relation between the two is given by a power series in α_s:

$$m_{b,PS}(\mu) \;=\; m_{b,1S} - \frac{4\alpha_s(\mu)}{3\pi}\mu + O(\alpha_s^2), \tag{7}$$

The difference between Beneke's values for $m_{b,1S}$ and $m_{b,PS}$ is mostly accounted for by the order-α_s correction. We will choose the 1S mass as our prescription for the b quark mass. Beneke's central value for the PS mass differs by 2 standard deviations from the 1S mass. This difference should not be regarded as an ambiguity in the quark mass, because it could not be eliminated by a more precise determination of m_b. Instead its effects on the cross section could be decreased by calculating the next-to-leading order radiative correction to the parton cross sections. The uncertainty due to different prescriptions for the quark mass can therefore be regarded as part of the error due to radiative corrections.

	$\langle O_1^{\Upsilon(nS)}(^3S_1)\rangle$				$\langle O_1^{\chi_{b0}(nP)}(^3P_0)\rangle$	
	phenomenology	potential models	lattice		potential models	lattice
$\Upsilon(3S)$	4.3 ± 0.9	3.7 ± 1.5	$9.6 \pm ?$	$\chi_b(3P)$	2.7 ± 0.7	
$\Upsilon(2S)$	4.5 ± 0.7	5.0 ± 1.8	$3.6 \pm ?$	$\chi_b(2P)$	2.6 ± 0.5	
$\Upsilon(1S)$	10.9 ± 1.6	10.8 ± 5.5	$7.6 \pm ?$	$\chi_b(1P)$	2.4 ± 0.4	$1.5 \pm ?$

TABLE II. Direct color-singlet matrix elements for Υ and χ_b states ($\langle O_1(^3S_1)\rangle$ in units of GeV^3, $\langle O_1(^3P_J)\rangle$ in units of GeV^5).

IV. COLOR-SINGLET MATRIX ELEMENTS

The color-singlet matrix elements for $\Upsilon(nS)$ can be determined phenomenologically from its decay rate into a lepton pair. The electronic decay rate of the $\Upsilon(nS)$, including the QCD radiative correction of order α_s and the first relativistic correction of order v^2, is

$$\Gamma[\Upsilon(nS) \to e^+e^-] \;=\; \frac{2\pi\alpha^2 e_b^2}{9m_b^2}\left(1 - \frac{8}{3}\frac{\alpha_s}{\pi} - \frac{1}{3}\frac{M_{\Upsilon(nS)} - 2m_b}{2m_b}\right)^2 \langle O_1^{\Upsilon(nS)}(^3S_1)\rangle, \tag{8}$$

where $e_b = -1/3$ is the bottom quark charge and m_b is the 1S mass. The relativistic correction was first expressed in terms of $M_{\Upsilon(nS)} - 2m_b$ by Gremm and Kapustin [12]. The vacuum saturation approximation, which is accurate up to corrections of order v^4, has been used to express the NRQCD matrix element that enters naturally in annihilation rates in terms of the corresponding production matrix element $\langle O_1^{\Upsilon(nS)}(^3S_1)\rangle$. It has also been used to express the radiative and relativistic correction factor as a square. Setting $m_b = 4.77$ GeV and $\alpha_s(m_b) = 0.22$ and using the measured value for the decay rates, we obtain the values for the color-singlet matrix elements in Table II. In addition to the experimental errors in the decay rates, there are theoretical errors from relativistic corrections and from perturbative corrections. As a measure of the relativistic error of order v^4, we take the square of the largest of the order-v^2 corrections for the three $\Upsilon(nS)$ states: $[(M_{\Upsilon(3S)} - 2m_b)/(3m_b)]^2 \approx 0.2\%$. As a measure of the perturbative error from higher orders in α_s, we take the square of the order-α_s correction in (8): $[16\alpha_s/(3\pi)]^2 \approx 14\%$. The error bars quoted in Table II are obtained by combining the experimental, relativistic, and perturbative errors in quadrature. The error bars are dominated by the 14% perturbative error, except in the case of the $\Upsilon(3S)$ for which the experimental error is 16%. The values for $\langle O_1^{\Upsilon(nS)}(^3S_1)\rangle$ in Table II are larger by a factor of 3 than those given in Table I of the first paper in Ref. [3] because of a normalization error in the Table. This normalization error did not appear in the cross sections and therefore did not affect the results.

There is no data that can be used for phenomenological determinations of the color-singlet matrix elements for the P-wave states. However the color-singlet matrix elements for both the S-wave and P-wave states can be estimated using wavefunctions from potential models. Using the vaccuum-saturation approximation, the color-singlet matrix element for $\Upsilon(nS)$ can be expressed in terms of its radial wavefunction at the origin, while that for $\chi_{bJ}(nP)$ can be expressed in terms of the derivative of its radial wavefunction at the origin:

	$\langle O_1(^3S_1)\rangle_{\rm inc}^{\Upsilon(nS)}$	$\langle O_1(^3P_0)\rangle_{\rm inc}^{\Upsilon(nS)}$	$\frac{1}{3}\langle O_1(^3P_1)\rangle_{\rm inc}^{\Upsilon(nS)}$	$\frac{1}{5}\langle O_1(^3P_2)\rangle_{\rm inc}^{\Upsilon(nS)}$
$\Upsilon(3S)$	4.3 ± 0.9	0 ?	0 ?	0 ?
$\Upsilon(2S)$	5.0 ± 0.7	0.12 ± 0.06	0.55 ± 0.15	0.42 ± 0.10
$\Upsilon(1S)$	12.8 ± 1.6	< 0.2	1.23 ± 0.25	0.84 ± 0.15

TABLE III. Inclusive color-singlet matrix elements for Υ states ($\langle O_1(^3S_1)\rangle$ in units of GeV^3, $\langle O_1(^3P_J)\rangle$ in units of GeV^5).

$$\langle O_1^{\Upsilon(nS)}(^3S_1)\rangle \approx \frac{9}{2\pi}|R_{\Upsilon(nS)}(0)|^2, \tag{9}$$

$$\langle O_1^{\chi_{bJ}(nP)}(^3P_J)\rangle \approx (2J+1)\frac{9}{2\pi}|R'_{\chi_b(nP)}(0)|^2. \tag{10}$$

Eichten and Quigg have tabulated the radial wavefunctions and their derivatives at the origin for 4 potential models that reproduce the observed bottomonium spectrum [13]. As estimates of the color-singlet matrix elements (9) and (10), we take the mean values from the 4 potential models in Ref. [13]. The mean values are tabulated in Table II. The errors are the root-mean-square deviations of the 4 potential-model values. The potential model estimates of $\langle O_1^{\Upsilon(nS)}(^3S_1)\rangle$ are consistent with the phenomenological values, but have larger error bars. This gives us some confidence in the potential-model estimates for $\langle O_1^{\chi_{b0}(nP)}(^3P_0)\rangle$ in Table II. These values are consistent within errors with those used in the analysis of Ref. [3].

The most accurate determination of the color-singlet matrix elements for the lowest bottomonium states may eventually come from lattice gauge theory. The corresponding annihilation matrix elements can be readily calculated using lattice simulations of NRQCD [14]. The NRQCD collaboration has calculated the wavefunctions for the lowest S-wave states [14] and P-wave states [15] of bottomonium. Inserting these wavefunctions into the expressions in (9) and (10), we obtain the estimates of the color-singlet matrix elements in Table II. The largest errors in the lattice calculations come from matching of lattice NRQCD operators with continuum NRQCD operators and from the omission of dynamical light quarks. Both errors could be as large as 25% in the present calculations. It is premature to quote error bars for the lattice gauge theory results in Table II.

We will adopt the phenomenological values of $\langle O_1^{\Upsilon(nS)}(^3S_1)\rangle$ in Table II and the potential-model values for $\langle O_1^{\chi_{b0}(nP)}(^3S_1)\rangle$. Using the branching fractions in Table I, we can form the linear combinations that appear in the expressions (4) for the inclusive $\Upsilon(nS)$ cross sections. These are tabulated in Table III. As indicated by the zeros in the first row, we neglect feeddown from the $\chi_b(3P)$ states.

V. COLOR-OCTET MATRIX ELEMENTS

The color-octet NRQCD matrix elements are phenomenological parameters that can only be determined from experimental data. We first extract the inclusive color-octet matrix elements for $\Upsilon(nS)$ from the CDF measurements of the inclusive $\Upsilon(nS)$ cross sections. We

then extract direct color-octet matrix elements for $\chi_{bJ}(nP)$ from the CDF measurements of the fraction of $\Upsilon(1S)$ coming from χ_b's. This gives us enough information to determine the direct color-octet matrix elements for $\Upsilon(nS)$.

A. Inclusive Matrix Elements for S-waves

The inclusive $\Upsilon(nS)$ cross sections depend linearly on the inclusive matrix elements defined in (5). The inclusive color-singlet matrix elements are given in Table III. We can extract the inclusive color-octet matrix elements from the CDF measurements of the $\Upsilon(nS)$ cross sections [4]. The differential cross sections integrated over rapidities $|y| < 0.4$ have been measured out to $p_T = 20$ GeV [4]. The CDF data on $Bd\sigma/dp_T$ for $\Upsilon(nS)$, where B is the branching fraction for $\Upsilon(nS) \to \mu^+\mu^-$, are shown in Figures 1, 2, and 3 for $\Upsilon(1S)$, $\Upsilon(2S)$, and $\Upsilon(3S)$, respectively. We avoid the problem of carrying out soft-gluon resummation to determine the shapes of the theoretical p_T distributions at low p_T by using only the data from $p_T > 8$ GeV to fit the color-octet matrix elements. This leaves 5 p_T bins for $\Upsilon(1S)$ and 3 p_T bins each for $\Upsilon(2S)$ and $\Upsilon(3S)$.

The inclusive $\Upsilon(nS)$ cross sections depend on the inclusive color-octet matrix elements through the linear combination $[\langle O_8(^1S_0)\rangle + m\ \langle O_8(^3P_0)\rangle/m_b^2] + n\ \langle O_8(^3S_1)\rangle$, where m varies from 4.6 at $p_T = 8$ GeV to 3.4 at $p_T = 20$ GeV, while n varies from 1.0 at $p_T = 8$ GeV to 6.3 at $p_T = 20$ GeV. The parameters $\langle O_8(^1S_0)\rangle$ and $\langle O_8(^3P_0)\rangle$ can not be determined independently, because the corresponding parton cross sections have similar dependences on p_T. We therefore carry out our analysis under the two extreme assumptions that either the $\langle O_8(^1S_0)\rangle$ term or the $\langle O_8(^3P_0)\rangle$ term dominates and that the other can be neglected. Assuming both matrix elements are positive, the truth will be somewhere in between the two extremes. We will take the difference between the two extremes as part of the theoretical error.

For a given choice of the parton distributions and the scales μ_F and μ_R, we can integrate the $\Upsilon(nS)$ differential cross section (4) over $|y| < 0.4$ and over each p_T bin. We determine the best fits for the color-octet matrix elements by minimizing the χ^2 associated with the sum over p_T bins. Fixing $\mu_F = \mu_R = \mu_T$ and assuming that $\langle O_8(^3P_0)\rangle$ is negligible, we obtain the values of $\langle O_8(^3S_1)\rangle$ and $\langle O_8(^1S_0)\rangle$ in the 1st and 3rd columns of Table IV. Repeating the analysis but assuming that $\langle O_8(^1S_0)\rangle$ is negligible, we obtain the values of $\langle O_8(^3S_1)\rangle$ and $\langle O_8(^3P_0)\rangle$ in the 2nd and 4th columns. The first errors in Table IV are extracted from the matrix of second derivatives of the χ^2 function. There is also an error from varying the renormalization and factorization scales μ_F and μ_R. These errors are large, but since they are highly correlated, we have separated them out as a second error in Table IV. The upper and lower errors are the shifts in the matrix elements that minimize χ^2 when μ_R and μ_F are changed from the central value $\mu_T = \sqrt{m_b^2 + p_T^2}$ by multiplicative factors of 2 and 1/2, respectively. The error from varying m_b is also highly correlated, but it is smaller and we do not list it separately. It can be taken into account when we use the matrix elements to calculate other observables.

Our fits for $Bd\sigma/dp_T dy$ at $y = 0$ for inclusive $\Upsilon(1S)$, $\Upsilon(2S)$, and $\Upsilon(3S)$ are compared to the CDF data in Figures 1, 2, and 3. The error bands reflect the statistical uncertainties in the matrix elements. The fits are reasonably good in the region $p_T > 8$ GeV that we used for fitting. At low p_T, our fits for $d\sigma/dp_T$ behave like $1/p_T$, because we have not implemented

	CTEQ5L		MRSTLO	
$\langle O_8(^3S_1)\rangle_{\rm inc}^{\Upsilon(3S)}$	$3.6 \pm 1.9^{+1.8}_{-1.3}$	$3.9 \pm 1.7^{+2.0}_{-1.4}$	$3.7 \pm 2.1^{+1.7}_{-1.3}$	$4.1 \pm 1.9^{+1.9}_{-1.4}$
$\langle O_8(^1S_0)\rangle_{\rm inc}^{\Upsilon(3S)}$	$5.4 \pm 4.3^{+3.1}_{-2.2}$	0	$7.5 \pm 4.9^{+3.4}_{-2.5}$	0
$\frac{5}{m_b^2}\langle O_8(^3P_0)\rangle_{\rm inc}^{\Upsilon(3S)}$	0	$5.7 \pm 4.6^{+3.3}_{-2.3}$	0	$7.9 \pm 5.2^{+3.7}_{-2.6}$
$\langle O_8(^3S_1)\rangle_{\rm inc}^{\Upsilon(2S)}$	$18.0 \pm 5.6^{+8.9}_{-6.4}$	$17.2 \pm 5.0^{+8.7}_{-6.2}$	$19.6 \pm 6.3^{+8.9}_{-6.5}$	$19.0 \pm 5.6^{+8.7}_{-6.4}$
$\langle O_8(^1S_0)\rangle_{\rm inc}^{\Upsilon(2S)}$	$-10.2 \pm 9.7^{-3.1}_{+1.8}$	0	$-8.7 \pm 11.1^{-2.4}_{+1.8}$	0
$\frac{5}{m_b^2}\langle O_8(^3P_0)\rangle_{\rm inc}^{\Upsilon(2S)}$	0	$-10.6 \pm 10.2^{-3.0}_{+2.2}$	0	$-8.9 \pm 11.7^{-2.5}_{+1.8}$
$\langle O_8(^3S_1)\rangle_{\rm inc}^{\Upsilon(1S)}$	$11.6 \pm 2.7^{+5.9}_{-4.2}$	$12.4 \pm 2.5^{+6.6}_{-4.7}$	$11.7 \pm 3.0^{+5.7}_{-4.2}$	$13.0 \pm 2.8^{+6.4}_{-4.7}$
$\langle O_8(^1S_0)\rangle_{\rm inc}^{\Upsilon(1S)}$	$10.9 \pm 6.2^{+10.2}_{-7.1}$	0	$18.1 \pm 7.2^{+11.4}_{-8.1}$	0
$\frac{5}{m_b^2}\langle O_8(^3P_0)\rangle_{\rm inc}^{\Upsilon(1S)}$	0	$11.1 \pm 6.5^{+10.7}_{-7.5}$	0	$18.6 \pm 7.5^{+11.9}_{-8.4}$

TABLE IV. Inclusive color-octet matrix elements for Υ states (in units of 10^{-2} GeV^3).

the effects of soft-gluon radiation on the shape of the p_T-distribution. The fits therefore diverge from the data below $p_T = 8$ GeV. For $\Upsilon(2S)$, the central curve becomes negative at small p_T because our fit gives a negative central value for $\langle O_8(^1S_0)\rangle_{\rm inc}^{\Upsilon(2S)}$ or $\langle O_8(^3P_0)\rangle_{\rm inc}^{\Upsilon(2S)}$. If we had fit the color-octet matrix elements using the data for $p_T > 4$ GeV, instead of only the data for $p_T > 8$ GeV, the central values for $\langle O_8(^1S_0)\rangle_{\rm inc}$ or $\langle O_8(^3P_0)\rangle_{\rm inc}$ would also have been negative for $\Upsilon(1S)$ and $\Upsilon(3S)$.

In Figures 1, 2, and 3, the color-singlet model predictions from order-α_s^3 fusion processes are shown as dashed lines. At the largest values of p_T shown, the predictions fall more than an order of magnitude below the data. The color-singlet model prediction for $\Upsilon(3S)$ indicates the shape of the $b\bar{b}_1(^3S_1)$ cross section. The color-singlet model predictions for $\Upsilon(1S)$ and $\Upsilon(2S)$ behave very differently at small p_T, because they receive contributions from decays of $\chi_{bJ}(nP)$. The predictions diverge as $p_T \to 0$, because the cross sections $d\hat{\sigma}/dp_T$ for $b\bar{b}_1(^3P_{0,2})$ behave like $1/p_T$. In order to obtain the correct threshold behavior in these channels, it would be necessary to resum the effects of soft-gluon radiation.

B. Direct Matrix Elements for P-waves

The color-octet matrix elements $\langle O_8(^3S_1)\rangle$ for the χ_b's can be determined from CDF measurements of the fractions of $\Upsilon(1S)$'s that come from $\chi_b(1P)$'s and from $\chi_b(2P)$'s [5]. The important feeddown decays for $\chi_{bJ}(1P)$ and $\chi_{bJ}(2P)$ proceed through the $\Upsilon(2S)$ and $\Upsilon(3S)$, respectively. The fractions $F_{\chi_b(nP)}^{\Upsilon(1S)}$ of $\Upsilon(1S)$'s from $\chi_b(nP)$ therefore satisfy

$$F_{\chi_b(1P)}^{\Upsilon(1S)}\ \sigma[\Upsilon(1S)]_{\rm inc} = \sum_J B_{\chi_{bJ}(1P)\to\Upsilon(1S)}\ \sigma[\chi_{bJ}(1P)] + \left(\sum_J B_{\Upsilon(2S)\to\chi_{bJ}(1P)} B_{\chi_{bJ}(1P)\to\Upsilon(1S)}\right) \sigma[\Upsilon(2S)]_{\rm inc}, \tag{11}$$

$$F_{\chi_b(2P)}^{\Upsilon(1S)}\ \sigma[\Upsilon(1S)]_{\rm inc} = \sum_J B_{\chi_{bJ}(2P)\to\Upsilon(1S)}\ \sigma[\chi_{bJ}(2P)]$$

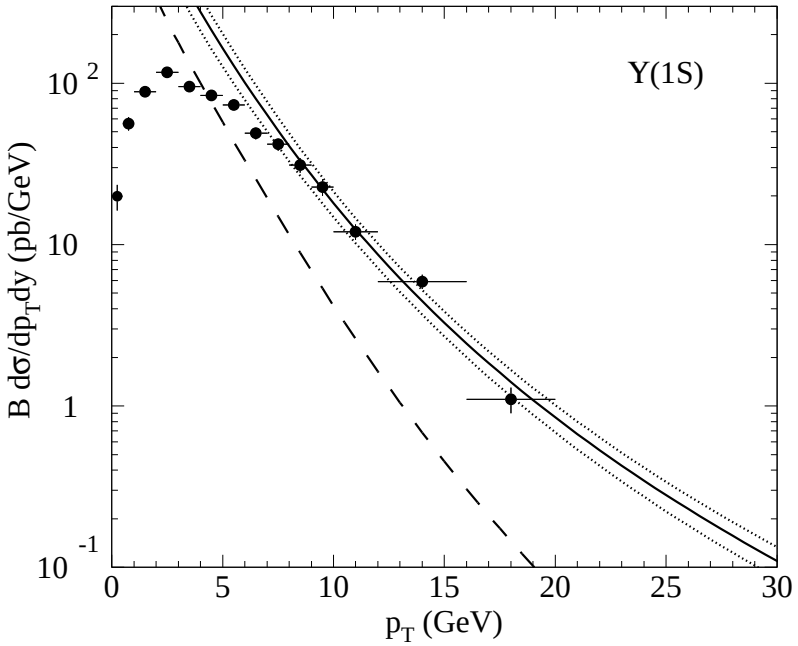

FIG. 1. Inclusive cross section for $\Upsilon(1S)$ at $y = 0$ in Run I multiplied by its branching fraction B into $\mu^+\mu^-$ as a function of p_T: CDF data, NRQCD fit (solid line) with statistical error bars (dotted lines), and color-singlet model prediction (dashed line).

$$+\left(\sum_J B_{\Upsilon(3S)\to\chi_{bJ}(2P)} B_{\chi_{bJ}(2P)\to\Upsilon(1S)}\right)\sigma[\Upsilon(3S)]_{\rm inc}. \tag{12}$$

Using the branching fractions from Table I, the coefficients of $\sigma[\Upsilon(2S)]_{\rm inc}$ and $\sigma[\Upsilon(3S)]_{\rm inc}$ in (11) and (12) are $(3.8 \pm 0.7)\%$ and $(1.8 \pm 0.2)\%$, respectively.

The CDF result for the fractions of $\Upsilon(1S)$'s with $|y| < 0.4$ and $p_T > 8$ GeV that come from $\chi_b(1P)$'s and $\chi_b(2P)$'s are

$$F^{\Upsilon(1S)}_{\chi_b(1P)} = (27.1 \pm 8.1)\%, \tag{13}$$

$$F^{\Upsilon(1S)}_{\chi_b(2P)} = (10.5 \pm 4.8)\%, \tag{14}$$

where we have added the statistical and systematic errors in quadrature. The inclusive $\Upsilon(nS)$ cross sections in (11) and (12) are the cross sections integrated over $|y| < 0.4$ and $p_T > 8$ GeV. Using the CDF measurements of these cross sections, (13) and (14) reduce to the following constraints on the cross sections for $\chi_{bJ}(1P)$ and $\chi_{bJ}(2P)$:

$$\sum_J B_{\chi_{bJ}(nP)\to\Upsilon(1S)}\,\sigma[\chi_{bJ}(nP)] = (0.85 \pm 0.29)\ {\rm nb}, \qquad n = 1, \tag{15}$$

$$= (0.34 \pm 0.17)\ {\rm nb}, \qquad n = 2. \tag{16}$$

The branching fractions and the associated errors are given in Table I.

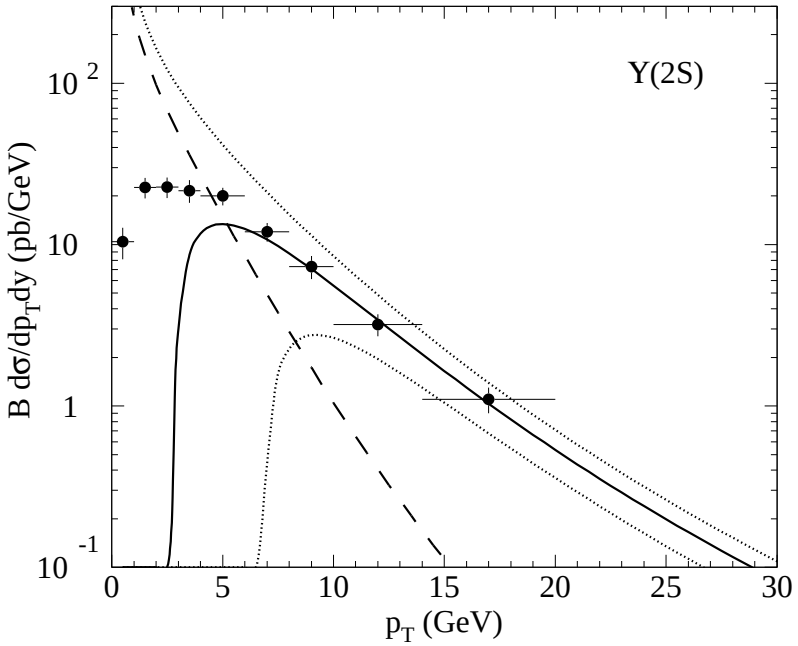

FIG. 2. Inclusive cross section for $\Upsilon(2S)$ at $y = 0$ in Run I multiplied by its branching fraction B into $\mu^+\mu^-$ as a function of p_T: CDF data, NRQCD fit, and color-singlet model prediction.

The theoretical cross sections for $\sigma[\chi_{bJ}(nP)]$, $J = 0, 1, 2$, are obtained by integrating (3) over the appropriate region of y and p_T. The constraints (15) and (16) are then linear equations for $\langle O_8^{\chi_{b0}(nP)}(^3S_1)\rangle$, which give the values in Table V. The first error is obtained by setting $\mu_F = \mu_R = \mu_T$ and combining in quadrature the experimental error from (15) or (16), the error from the branching fractions in Table I, and the errors from the color-singlet matrix elements in Table II. The second upper and lower errors in Table V are the shifts in the matrix elements when μ_R and μ_F are changed from their central values by multiplicative factors of 2 and 1/2, respectively.

C. Direct Matrix Elements for S-waves

The NRQCD matrix elements in Table IV can be used to calculate the inclusive $\Upsilon(nS)$ cross sections. To calculate the direct $\Upsilon(nS)$ cross sections, we must extract direct color-octet matrix elements for the $\Upsilon(nS)$ states from the inclusive color-octet matrix elements given in Table IV. The linear combinations of matrix elements determined by the inclusive $\Upsilon(1S)$ cross sections are

$$\langle O_8(^3S_1)\rangle_{\rm inc}^{\Upsilon(1S)} = \langle O_8^{\Upsilon(1S)}(^3S_1)\rangle + 0.311\ \langle O_8^{\Upsilon(2S)}(^3S_1)\rangle + 0.112\ \langle O_8^{\Upsilon(3S)}(^3S_1)\rangle + 2.15\ \langle O_8^{\chi_{b0}(1P)}(^3S_1)\rangle + 1.08\ \langle O_8^{\chi_{b0}(2P)}(^3S_1)\rangle, \quad (17)$$

$$\langle O_8(^1S_0)\rangle_{\rm inc}^{\Upsilon(1S)} = \langle O_8^{\Upsilon(1S)}(^1S_0)\rangle + 0.311\ \langle O_8^{\Upsilon(2S)}(^1S_0)\rangle + 0.112\ \langle O_8^{\Upsilon(3S)}(^1S_0)\rangle, \quad (18)$$

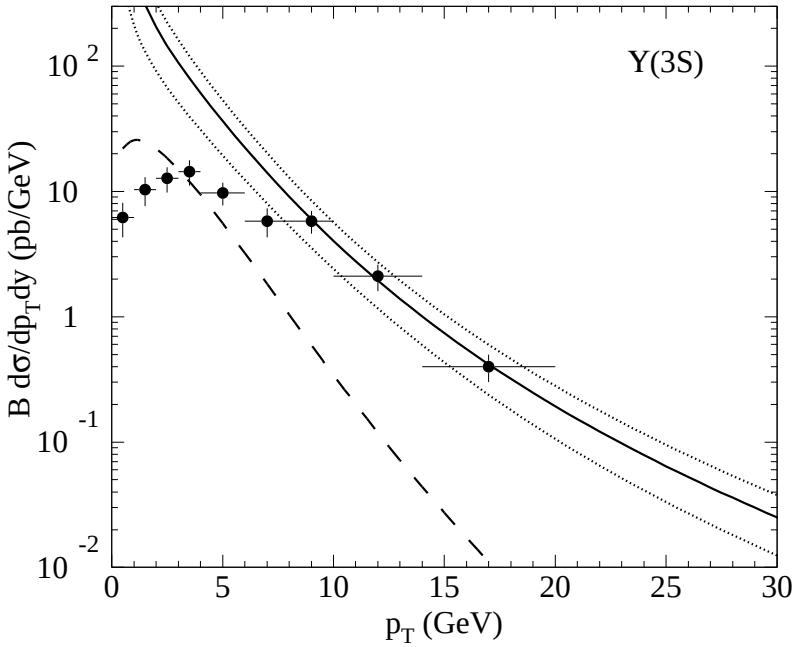

FIG. 3. Inclusive cross section for $\Upsilon(3S)$ at Run I multiplied by its branching fraction B into $\mu^+\mu^-$ as a function of p_T: CDF data, NRQCD fit, and color-singlet model prediction.

$$\langle O_8(^3P_0)\rangle_{\rm inc}^{\Upsilon(1S)} = \langle O_8^{\Upsilon(1S)}(^3P_0)\rangle + 0.311\ \langle O_8^{\Upsilon(2S)}(^3P_0)\rangle + 0.112\ \langle O_8^{\Upsilon(3S)}(^3P_0)\rangle. \tag{19}$$

The errors on the branching fractions in (17)–(19) have been suppressed, but they are (0.311 ± 0.016), (0.112 ± 0.005), (2.15 ± 0.31), and (1.08 ± 0.08). The linear combinations determined by the inclusive $\Upsilon(2S)$ cross sections are

$$\langle O_8(^3S_1\rangle_{\rm inc}^{\Upsilon(2S)} = \langle O_8^{\Upsilon(2S)}(^3S_1)\rangle + 0.106\ \langle O_8^{\Upsilon(3S)}(^3S_1)\rangle + 1.49\ \langle O_8^{\chi_{b0}(2P)}(^3S_1)\rangle, \tag{20}$$

$$\langle O_8(^1S_0)\rangle_{\rm inc}^{\Upsilon(2S)} = \langle O_8^{\Upsilon(2S)}(^1S_0)\rangle + 0.106\ \langle O_8^{\Upsilon(3S)}(^1S_0)\rangle, \tag{21}$$

$$\langle O_8(^3P_0)\rangle_{\rm inc}^{\Upsilon(2S)} = \langle O_8^{\Upsilon(2S)}(^3P_0)\rangle + 0.106\ \langle O_8^{\Upsilon(3S)}(^3P_0)\rangle. \tag{22}$$

The errors on the branching fractions in (20)–(22) are (0.106 ± 0.008) and (1.49 ± 0.17). Using the color-octet matrix elements for inclusive $\Upsilon(nS)$ in Table IV and the color-octet matrix elements for direct $\chi_b(nP)$ in Table V, we obtain the color-octet matrix elements for direct $\Upsilon(nS)$ in Table V.

Our analysis gives a negative value consistent with zero for the matrix elements $\langle O_8^{\Upsilon(2S)}(^1S_0)\rangle$ or $\langle O_8^{\Upsilon(2S)}(^3P_0)\rangle$. Our values for $\langle O_8^{\chi_{b0}(2P)}(^3S_1)\rangle$, $\langle O_8^{\chi_{b0}(1P)}(^3S_1)\rangle$, and $\langle O_8^{\Upsilon(1S)}(^3S_1)\rangle$ are also consistent with zero given the statistical error. The only direct color-octet matrix elements that differ from zero by two or more statistical error bars are $\langle O_8^{\Upsilon(2S)}(^3S_1)\rangle$ and $\langle O_8^{\Upsilon(1S)}(^1S_0)\rangle$ or $\langle O_8^{\Upsilon(1S)}(^3P_0)\rangle$.

We now compare our values for the matrix elements with those obtained by Cho and Leibovich in their pioneering analysis of bottomonium production at the Tevatron. Their

	CTEQ5L		MRSTLO	
$\langle O_8^{\chi_{b0}(2P)}(^3S_1)\rangle$	$0.8 \pm 1.1^{+1.1}_{-0.8}$		$1.2 \pm 1.3^{+1.1}_{-0.8}$	
$\langle O_8^{\chi_{b0}(1P)}(^3S_1)\rangle$	$1.5 \pm 1.1^{+1.3}_{-1.0}$		$1.9 \pm 1.3^{+1.4}_{-1.0}$	
$\langle O_8^{\Upsilon(2S)}(^3S_1)\rangle$	$16.4 \pm 5.7^{+7.1}_{-5.1}$	$15.6 \pm 5.2^{+6.9}_{-4.9}$	$17.4 \pm 6.4^{+7.0}_{-5.1}$	$16.8 \pm 5.8^{+6.8}_{-5.0}$
$\langle O_8^{\Upsilon(2S)}(^1S_0)\rangle$	$-10.8 \pm 9.7^{-3.4}_{+2.0}$	0	$-9.5 \pm 11.1^{-2.8}_{+2.1}$	0
$\frac{5}{m_b^2}\langle O_8^{\Upsilon(2S)}(^3P_0)\rangle$	0	$-11.2 \pm 10.2^{-3.3}_{+2.4}$	0	$-9.7 \pm 11.6^{-2.9}_{+2.1}$
$\langle O_8^{\Upsilon(1S)}(^3S_1)\rangle$	$2.0 \pm 4.1^{-0.6}_{+0.5}$	$3.0 \pm 3.8^{+0.2}_{-0.1}$	$0.4 \pm 4.7^{-1.0}_{+0.7}$	$1.8 \pm 4.4^{-0.2}_{+0.1}$
$\langle O_8^{\Upsilon(1S)}(^1S_0)\rangle$	$13.6 \pm 6.8^{+10.8}_{-7.5}$	0	$20.2 \pm 7.8^{+11.9}_{-8.5}$	0
$\frac{5}{m_b^2}\langle O_8^{\Upsilon(1S)}(^3P_0)\rangle$	0	$13.9 \pm 7.1^{+11.4}_{-8.0}$	0	$20.7 \pm 8.1^{+12.4}_{-8.8}$

TABLE V. Direct color-octet matrix elements for χ_b and Υ states (in units of 10^{-2} GeV^3).

analysis was based on the CDF data sample from Run IA of the Tevatron [2]. To reduce the errors associated with the shape of the p_T distribution at small p_T, they used only the data from $p_T > 3.5$ GeV in their analysis. The data was insufficient to determine all the matrix elements, so they estimated the matrix elements $\langle O_8^{\Upsilon(nS)}(^3S_1)\rangle$ by applying scaling relations to the corresponding matrix elements in the charmonium sector. Their value for $\langle O_8^{\Upsilon(1S)}(^3S_1)\rangle$ is consistent with ours to within our large error bars, but their value for $\langle O_8^{\Upsilon(2S)}(^3S_1)\rangle$ is smaller than ours by about a factor of 40. They used the CDF data to fit the matrix elements $\langle O_8^{\chi_b(nP)}(^3S_1)\rangle$ and the linear combinations $M_5^{\Upsilon(nS)} = \langle O_8^{\Upsilon(nS)}(^1S_0)\rangle + 5\langle O_8^{\Upsilon(nS)}(^3P_0)\rangle/m_b^2$. Their values for $\langle O_8^{\chi_b(nP)}(^3S_1)\rangle$ are comparable to ours in magnitude, but they have much smaller error bars. Their values for $M_5^{\Upsilon(nS)}$ differ from zero by only about one error bar. In our analysis, we included the matrix elements $\langle O_8^{\Upsilon(nS)}(^3S_1)\rangle$ in the list of those to be fit to the CDF data. The much higher quality of the CDF data from Run IB of the Tevatron [4] allowed us to carry out a reasonable fit using the data restricted to $p_T > 8$ GeV.

VI. INCLUSIVE CROSS SECTIONS FOR SPIN-TRIPLET STATES

Having determined the most important matrix elements for the production of the spin-triplet bottomonium states, we can use them to calculate the cross sections for these states in other high energy processes. In particular, we can calculate their cross sections in Run II of the Tevatron in which the center-of-mass energy will be increased from 1.8 TeV to 2.0 TeV. In order to cancel the large theoretical errors, such as those from the uncertainties in the matrix elements and from the choice of scale, we normalize the cross sections to that for inclusive $\Upsilon(1S)$ at $\sqrt{s} = 1.8$ TeV. For each bottomonium state H, we define the ratio

$$R^H(\sqrt{s}) = \frac{\sigma[H;\ \sqrt{s}]}{\sigma[\text{inclusive } \Upsilon(1S);\ \sqrt{s} = 1.8 \text{ TeV}]}, \tag{23}$$

where the cross sections are integrated over $p_T > 8$ GeV and over $|y| < 0.4$.

H	R^H(1.8 TeV)	R^H(2.0 TeV)
$\Upsilon(3S)$	0.31 ± 0.14	0.36 ± 0.16
$\chi_{b2}(2P)$	0.44 ± 0.26	0.52 ± 0.30
$\chi_{b1}(2P)$	0.34 ± 0.16	0.39 ± 0.19
$\chi_{b0}(2P)$	0.20 ± 0.07	0.24 ± 0.08
$\Upsilon(2S)$	0.65 ± 0.35	0.76 ± 0.41
$\chi_{b2}(1P)$	0.57 ± 0.26	0.66 ± 0.31
$\chi_{b1}(1P)$	0.41 ± 0.17	0.48 ± 0.19
$\chi_{b0}(1P)$	0.23 ± 0.08	0.26 ± 0.09
$\Upsilon(1S)$	1	1.16 ± 0.01

TABLE VI. Ratios of the inclusive cross sections for the spin-triplet bottomonium states H at the Tevatron with $\sqrt{s} = 1.8$ TeV and 2.0 TeV to the inclusive cross section for $\Upsilon(1S)$ with $\sqrt{s} = 1.8$ TeV.

To calculate the inclusive cross section for $\Upsilon(nS)$, we simply use the inclusive color-singlet matrix elements from Table III and the inclusive color-octet matrix elements from Table IV. To calculate the inclusive cross section for $\chi_{bJ}(nP)$, we must first compute the direct cross sections for $\chi_{bJ}(nP)$ and the higher bottomonium states using the direct color-singlet matrix elements from Table II and the direct color-octet matrix elements from Table V, and then combine them using the inclusive branching fractions in Table I. The resulting ratios R^H shown in Table VI are the averages of the 4 values obtained by using either the CTEQ5L or MRST98LO parton distributions and either setting $\langle O_8(^1S_0)\rangle = 0$ or $\langle O_8(^3P_0)\rangle = 0$. The error bars come from combining in quadrature the statistical errors in the matrix elements from the Tables, the error from varying μ by a factor of two from its central value, the difference between using the CTEQ5L and MRST98LO parton distributions, the difference between setting $\langle O_8(^1S_0)\rangle = 0$ and $\langle O_8(^3P_0)\rangle = 0$, and the error from varying m_b. The error bars in the numerator and denominator of (23) are both large, but they are highly correlated and tend to cancel in the ratio. The largest contributions to the error bars are the statistical errors on the matrix elements, with the exception of $\Upsilon(1S)$, for which the largest contribution comes from varying the scale. For $\Upsilon(2S)$ and $\Upsilon(3S)$, the results in Table VI for $\sqrt{s} = 1.8$ TeV are consistent with the actual CDF measurements, which give 0.61 ± 0.12 for $\Upsilon(2S)$ and 0.29 ± 0.12 for $\Upsilon(3S)$. When the center-of-mass energy is increased from 1.8 TeV to 2.0 TeV, all the cross sections increase by about 16%. The increase depends on p_T, changing from about 15% at $p_T = 8$ TeV to about 19% at $p_T = 20$ TeV.

VII. DIRECT CROSS SECTIONS FOR SPIN-SINGLET STATES

Having determined the most important matrix elements for the production of the spin-triplet bottomonium states, we can also use them to calculate the production rate of the spin-singlet states $\eta_b(nS)$ and $h_b(nP)$. The matrix elements for these states are related to those of the corresponding spin-triplet states by the approximate spin symmetry of NRQCD. Spin symmetry relates the matrix elements for $\eta_b(nS)$ to those for $\Upsilon(nS)$:

$$\langle O_1^{\eta_b(nS)}({}^1S_0)\rangle = \frac{1}{3}\langle O_1^{\Upsilon(nS)}({}^3S_1)\rangle, \tag{24}$$

$$\langle O_8^{\eta_b(nS)}({}^1P_1)\rangle = \frac{1}{3}\langle O_8^{\Upsilon(nS)}({}^3P_0)\rangle, \tag{25}$$

$$\langle O_8^{\eta_b(nS)}({}^1S_0)\rangle = \frac{1}{3}\langle O_8^{\Upsilon(nS)}({}^3S_1)\rangle, \tag{26}$$

$$\langle O_8^{\eta_b(nS)}({}^3S_1)\rangle = \frac{1}{3}\langle O_8^{\Upsilon(nS)}({}^1S_0)\rangle. \tag{27}$$

The direct matrix elements for $\eta_b(nS)$ can therefore be read off from those for $\Upsilon(nS)$ in Tables II and V. The spin-symmetry relations have been used to calculate the cross sections for producing the η_c at the Tevatron [16], in photoproduction and electroproduction, [17], and at Hera-B [18]. In Refs. [16] and [17], the factor of $\frac{1}{3}$ which comes from the number of spin states was omitted from the spin-symmetry relations (24)-(27). Thus their estimates of the cross sections may be too large by a factor of 3. Spin symmetry relates the matrix elements for $h_b(nP)$ to those for $\chi_{b0}(nP)$:

$$\langle O_1^{h_b(nP)}({}^1P_1)\rangle = 3\langle O_1^{\chi_{b0}(nP)}({}^3P_0)\rangle, \tag{28}$$

$$\langle O_8^{h_b(nP}({}^1S_0)\rangle = 3\langle O_8^{\chi_{b0}(nP)}({}^3S_1)\rangle. \tag{29}$$

The direct matrix elements for $h_b(nP)$ can therefore be read off from those for $\chi_b(nP)$ in Tables II and V. These relations were first used by Fleming and Mehen to calculate the cross section for the photoproduction of h_c [19]. They have also been used to calculate the cross sections for h_c at Hera-B [18].

To calculate the cross sections for the direct production of the spin-singlet states at the Tevatron, we need the appropriate parton differential cross sections $d\hat{\sigma}$. Explicit expressions for most of those that are needed are given in Ref. [3] and in Ref. [9]. The exception is the cross sections for producing $b\bar{b}_8({}^1P_1)$, which contributes to η_b production. The cross sections for the production of $b\bar{b}_8({}^1P_1)$ in $q\bar{q}$, gq, and gg scattering are

$$\frac{d\sigma}{d\hat{t}}\left(q\bar{q} \to {}^1P_1^{(8)}g\right) = \frac{\langle O_8({}^1P_1)\rangle}{16\pi\hat{s}^2}\frac{4(4\pi\alpha_s)^3}{9M^3}\frac{\hat{t}^2+\hat{u}^2}{\hat{s}(\hat{s}-M^2)^2}, \tag{30}$$

$$\frac{d\sigma}{d\hat{t}}\left(gq \to {}^1P_1^{(8)}q\right) = \frac{\langle O_8({}^1P_1)\rangle}{16\pi\hat{s}^2}\frac{(4\pi\alpha_s)^3}{6M^3}\frac{\hat{s}^2+\hat{u}^2}{(-\hat{t})(M^2-\hat{t})^2}, \tag{31}$$

$$\begin{aligned}\frac{d\sigma}{d\hat{t}}\left(gg \to {}^1P_1^{(8)}g\right) = {}& \frac{\langle O_8({}^1P_1)\rangle}{16\pi\hat{s}^2}\frac{(4\pi\alpha_s)^3}{36M^3}\frac{1}{z^2\hat{s}(\hat{s}-M^2)^3(\hat{s}M^2+z^2)^3}\\ &\Big\{27\hat{s}z^2(\hat{s}^8-4\hat{s}^6z^2+\hat{s}^4z^4+\hat{s}^2z^6+z^8)\\ &+M^2(27\hat{s}^{10}-243\hat{s}^8z^2+697\hat{s}^6z^4-665\hat{s}^4z^6+346\hat{s}^2z^8-27z^{10})\\ &-M^4\hat{s}(135\hat{s}^8-702\hat{s}^6z^2+1340\hat{s}^4z^4-1087\hat{s}^2z^6+135z^8)\\ &+M^6(324\hat{s}^8-1134\hat{s}^6z^2+1557\hat{s}^4z^4-698\hat{s}^2z^6+54z^8)\\ &-M^8\hat{s}(486\hat{s}^6-1091\hat{s}^4z^2+882\hat{s}^2z^4-92z^6)\\ &+M^{10}(486\hat{s}^6-616\hat{s}^4z^2+374\hat{s}^2z^4-27z^6)\\ &-M^{12}\hat{s}(324\hat{s}^4-211\hat{s}^2z^2+38z^4)\\ &+M^{14}\hat{s}^2(135\hat{s}^2-38z^2)-27M^{16}\hat{s}^3\Big\}.\end{aligned} \tag{32}$$

H	R^H(1.8 TeV)	R^H(2.0 TeV)
$\eta_b(3S)$	1.72 ± 0.52	2.00 ± 0.61
$h_b(2P)$	0.07 ± 0.07	0.08 ± 0.09
$\eta_b(2S)$	1.77 ± 0.50	2.06 ± 0.59
$h_b(1P)$	0.11 ± 0.08	0.13 ± 0.09
$\eta_b(1S)$	4.31 ± 0.98	5.02 ± 1.14

TABLE VII. Ratios of the direct cross sections for the spin-singlet bottomonium states H at the Tevatron with $\sqrt{s} = 1.8$ TeV and 2.0 TeV to the inclusive cross section for $\Upsilon(1S)$ with $\sqrt{s} =$ 1.8 TeV.

where $z^2 = \hat{t}\hat{u}$.

We proceed to calculate the cross sections for the direct production of the spin-singlet states at the Tevatron at center-of-mass energies $\sqrt{s} = 1.8$ TeV and 2.0 TeV. To minimize the effect of the highly correlated errors, we calculate the ratio (23) of the direct cross section integrated over $p_T > 8$ GeV and over $|y| < 0.4$ to the corresponding inclusive cross section for $\Upsilon(1S)$ at 1.8 TeV. The resulting predictions are shown in Table VI. The cross sections for the $h_b(nP)$ states are small compared to those for $\Upsilon(1S)$ and they have large error bars. The cross sections for $\eta_b(nS)$ are predicted to be several times larger than those for $\Upsilon(nS)$ and they have reasonably small error bars. These predictions should be fairly reliable, because the cross sections are for the same kinematical region as the data used to extract the matrix elements. When the center-of-mass energy is increased from 1.8 TeV to 2 TeV, all the cross sections increase by about 16%.

We can make a rough estimate of the cross sections integrated over all p_T by assuming that the spin-singlet cross sections have the same shape at small p_T as the $\Upsilon(1S)$ cross section. The measured inclusive $\Upsilon(1S)$ cross section at central rapidity integrated over all p_T up to 20 GeV satisfies $Bd\sigma/dy = 690 \pm 25$ pb, where $B \approx 2.5\%$ is the branching fraction of $\Upsilon(1S)$ into $\mu^+\mu^-$. The cross section integrated only over $p_T > 8$ GeV satisfies $Bd\sigma/dy = 106 \pm 7$ pb. The ratio of these cross sections is 6.5 ± 0.5. Multiplying the inclusive $\Upsilon(1S)$ cross section $d\sigma/dy = 28$ nb by the factor of 6.5 to take into account the small p_T region and by the ratio 4.3 from Table VI, we find that the cross section for $\eta_b(1S)$ integrated over all p_T should be approximately $d\sigma/dy = 800$ nb.

The cross section for $\eta_b(1S)$ indicates that this state must have been produced in abundance in Run I of the Tevatron. However the $\eta_b(1S)$ can be observed only if it has a large enough branching fraction into a decay mode that can be triggered upon. One possibility is the double-J/ψ decay $\eta_b(1S) \to J/\psi + J/\psi$, followed by the decays $J/\psi \to \mu^+\mu^-$. The decay $\eta_b(1S) \to J/\psi + J/\psi$ has essentially the same kinematics as the decay $\eta_c \to \phi\phi$, except that all masses are scaled up by a factor of 3. Thus the branching fraction for $\eta_b(1S) \to J/\psi + J/\psi$ could be as large as that for $\eta_c \to \phi\phi$, which is approximately 7×10^{-3}. We can obtain a lower bound on the branching fraction by using the fact that in the limit $m_b \to \infty$ with m_c fixed, the branching fraction for $\eta_b(1S) \to J/\psi + J/\psi$ scales like $1/m_b^4$ [20]. If m_c and m_b were both in this scaling region, then the branching fraction into light $J^{PC} = 1^{--}$ mesons would be smaller for $\eta_b(1S)$ than for η_c by a factor of $(m_c/m_b)^4$, which is about 10^{-2}. Since we are not

deep into this scaling region, the suppression should be smaller than this. Thus the branching fraction for $\eta_b(1S) \to J/\psi + J/\psi$ should be in the range between 7×10^{-5} and 7×10^{-3}. Multiplying by the branching fractions of 6% for each of the decays $J/\psi \to \mu^+\mu^-$, our estimate for the branching fraction for $\eta_b(1S) \to J/\psi + J/\psi \to \mu^+\mu^- + \mu^+\mu^-$ is $B \approx 2.5 \times 10^{-6\pm1}$. The cross section for producing this particular decay mode of $\eta_b(1S)$ is therefore $B d\sigma/dy \approx 2$ pb, give or take a factor of 10. Multiplying by the rapidity interval 0.8 and by the integrated luminosity of about 100 pb^{-1} in Run I of the Tevatron, we obtain between 16 and 1600 produced events.

We must also take into account the acceptances and efficiencies for observing the decays $J/\psi \to \mu^+\mu^-$. These can be estimated using the CDF data on the production of prompt J/ψ in Run IA of the Tevatron [21]. Based on the observation of about 22,000 $J/\psi \to \mu^+\mu^-$ candidates with $p_T > 5$ GeV and pseudorapidity $|\eta| < 0.6$ in a 15 pb^{-1} data sample, they measured the cross section in that region of p_T and η to be $B\sigma \approx 17$ nb. We infer that the product of the acceptance and the efficiency is roughly $\epsilon \approx 0.09$. Multiplying the number of events that are produced by ϵ^2, we get between 0.13 and 13 observed events. Thus this cross section may be large enough to be observed in Run I of the Tevatron. In Run II, the integrated luminosity will be larger by a factor of 20 and there will be significant improvements in the acceptances and efficiencies for observing muons in both the CDF and D0 detectors. Thus the $\eta_b(1S)$ should certainly be observed in Run II through the decay $\eta_b \to J/\psi + J/\psi$.

VIII. DISCUSSION

We have carried out an updated NRQCD analysis of the CDF data on the production of spin-triplet bottomonium states from Run I of the Tevatron. In spite of using only the data from $p_T > 8$ GeV, we were able to extract all the relevant color-octet matrix elements directly from the data. Only one of the 8 color-octet matrix elements comes out with a negative central value, but several others are also consistent with zero to within errors. In our analysis, we distinguished between the inclusive color-octet matrix elements that can be used to compute inclusive $\Upsilon(nS)$ cross sections and the direct color-octet matrix elements required to compute direct $\Upsilon(nS)$ cross sections and, by spin symmetry, direct $\eta_b(nS)$ cross sections.

The most serious deficiency in our analysis was our failure to take into account the effects of soft-gluon radiation that are needed to give a smooth p_T distribution at small p_T. This forced us to use only the small fraction of the data from $p_T > 8$ GeV to fit the color-octet matrix elements, which led to large errors in these matrix elements. If these matrix elements are used to predict bottomonium cross sections in other high energy processes, the predictions will probably have large error bars. Our theoretical cross sections also diverge from the CDF data below $p_T = 8$ GeV, which gives us another reason to be cautious in applying our matrix elements to other high energy processes.

An analysis that deals properly with the small p_T region could take full advantage of the CDF data and therefore determine the color-octet matrix elements more accurately. Such an analysis requires a prescription for combining the leading-order cross sections for $ij \to b\bar{b} + k$ with the next-to-leading order cross sections for $ij \to b\bar{b}$ recently calculated by Petrelli et al. [22] to get a smooth p_T distribution near $p_T = 0$. The matrix elements extracted from such an

analysis should give reliable predictions for observables at the Tevatron that are dominated by low p_T. They should also give reliable predictions for bottomonium production in other high energy processes.

Our analysis should give reliable predictions for the cross sections of the spin-singlet states $\eta_b(nS)$ and $h_b(nP)$ at the Tevatron. We find that the direct cross section for $\eta_b(1S)$ at $p_T > 8$ GeV should be greater than the inclusive cross section for $\Upsilon(1S)$ by a factor of about 4.3. If we assume that the p_T distributions have the same shapes at smaller p_T, we can estimate the cross section for $\eta_b(1S)$ integrated over all p_T. The resulting cross section is large enough that it should be possible to discover the $\eta_b(1S)$ at the Tevatron if there is a decay mode with a large enough branching fraction that can be used as a trigger. We argued that the decay $\eta_b \to J/\psi + J/\psi$ should allow the discovery of the $\eta_b(1S)$, if not in the data from Run I, then certainly in Run II of the Tevatron.

ACKNOWLEDGMENTS

This work was supported in part by the U.S. Department of Energy under Grants DE-FG02-91-ER40690 and DOE-ER-40682-143 and by the Natural Sciences and Engineering Research Council of Canada. We thank F. Maltoni for valuable comments.

REFERENCES

[1] G.T. Bodwin, E. Braaten, and G.P. Lepage, Phys. Rev. D **51**, 1125 (1995).
[2] CDF Collaboration, Phys. Rev. Lett. **75**, 4358 (1997).
[3] P. Cho and A. Leibovich, Phys. Rev. D **53**, 150 (1996); Phys. Rev. D **53**, 6203 (1996).
[4] CDF Collaboration, CDF Note 5027.
[5] CDF Collaboration, CDF Note 4392; hep-ex/9910025.
[6] Particle Data Group, Eur. Phys. J. **C3**, 1 (1998).
[7] Y.-P. Kuang and T.-M. Yan, Phys. Rev. D **24**, 2874 (1981); Y.-P. Kuang, S.F. Tuan, and T.-M. Yan, Phys. Rev. D **37**, 1210 (1988).
[8] T.A. Lahde, C.J. Nyfalt, D.O. Riska, Nucl. Phys. **A645**, 587 (1999).
[9] M. Beneke, M. Krämer, and M. Vänttinen, Phys. Rev. D **57**, 4258 (1998).
[10] A.A. Penin and A.A Pivovarov, Nucl. Phys. **B549**, 217 (1999); Phys. Lett **B435**, 413 (1998); A. Hoang, Phys. Rev. D **61**, 034005 (2000); K. Melnikov and A. Yelkhovsky, Phys. Rev. D **59**, 114009 (1999); M. Beneke and A. Signer, Phys. Lett **B471**, 233 (1999); M. Beneke, A. Signer, and V.A. Smirnov, hep-ph/9906476.
[11] M. Beneke, hep-ph/9911490.
[12] M. Gremm and A. Kapustin, Phys. Lett. **B407**, 323 (1997).
[13] E. Eichten and C. Quigg, Phys. Rev. D **52**, 1726 (1995).
[14] C.T.H. Davies et al., Phys. Rev. D **58**, 054505 (1998).
[15] C.T.H. Davies and J. Shigemitsu (private communication).
[16] P. Mathews, P. Poulose, and K. Sridhar, Phys. Lett. **B438**, 336 (1998).
[17] L.-K. Hao, F. Yuan, and K.-T. Chao, Phys. Rev. Lett. **83**, 4490 (1999); hep-ph/0004203.
[18] C.-F. Qiao and C. Yuan, hep-ph/0005317.
[19] S. Fleming and T. Mehen, Phys. Rev. D **58**, 037503 (1998).
[20] S.J. Brodsky and G.P. Lepage, Phys. Rev. D **24**, 2848 (1981).
[21] CDF collaboration, Phys. Rev. Lett. **79**, 572 (1997).
[22] A. Petrelli, M. Cacciari, M. Greco, F. Maltoni, and M.L. Mangano, Nucl. Phys. **B514**, 245 (1998).